

Superhydrophobic Lubrication: Gas–Liquid Bilayer Reduces the Friction Between Two Solids

Heikki A. Nurmi, Cunming Yu, Dmytro Toptunov, Robin H.A. Ras,* and Ville Jokinen*

Lubrication is one of the most important ways to reduce the effect of friction, which is the single largest cause for energy losses in society. Typically, friction reduction is done by lubrication with petroleum-based oils, while technology focus is shifting toward environmentally-friendly green lubrication. Lowest friction coefficients with water-based lubrication have previously been achieved with smooth surfaces such as silicon carbide and silicon nitride or polyzwitterionic polymer brushes with typical coefficients of friction in the order of 0.002. Here, a novel concept for green lubrication using a bilayer of water and ambient air acting as the lubricant between a hydrophilic and superhydrophobic surface is shown. This method achieves superlubricity with friction coefficients down to 0.002 as measured with oscillating tribometer and tilting stage. In addition, possible applications for superhydrophobic lubrication such as tunable lubrication and a 2D mouse treadmill, are shown.

methods: lubricating fluids and solids, active and passive systems, and biomimetic and engineered systems. Typically, unlubricated and lubricated materials have friction coefficients μ between 1 and 0.01,^[1] and they can go down to 0.002 with ceramic bearings^[2] and hydrodynamical bearings.^[3] Extremely low friction coefficients have been reported for polymer brushes, from as low as 0.0004 at velocities of $\mu\text{m s}^{-1}$ ^[4] to 0.004 as the velocity reaches macroscopic values of 10 mm s^{-1} .^[5] Each lubrication method has its best performance limited to a specific range of pressure, velocity, and temperature. For example, hydrodynamic bearing with oil works best at MPa pressures, $\approx 1\text{ m s}^{-1}$ velocity and temperatures between $60\text{ }^\circ\text{C}$ and $80\text{ }^\circ\text{C}$. The lowest friction coefficients

1. Introduction

Friction between solid surfaces is a major cause of energy losses. Minimizing this energy loss has been a focus of study for a long time and there is a wide range of possible lubrication

(0.002) in commonly used bearings are with hydrodynamic bearings using oil as lubricant^[3,6] or ceramic bearings.^[2,7,8] Lubricants can be modified with additives for added corrosion resistance, improving anti-biofouling,^[9] and adjusting viscosity.^[6] One major consideration is the environmental friendliness of the lubricants.^[9] Pure water would be extremely friendly to the environment but water as a lubricant faces challenges. Journal bearings with water lubrication can reach $\mu \approx 0.01$ ^[10–12] and superlubricity ($\mu < 0.01$)^[13] has been achieved with water lubrication by using smooth self-mated silicon carbide (SiC) or silicon nitride (Si_3N_4) as the substrate. These lubrication systems can have friction coefficients as low as $\mu = 0.005$.^[7,8] These extremely low friction coefficients are due to boundary slipping between water and the smooth SiC or Si_3N_4 substrate with contact pressure of 300 MPa.


A liquid droplet in contact with a superhydrophobic solid surface shows very low adhesion and friction.^[14,15] Superhydrophobic surfaces are characterized by a contact angle larger than 150° , a low contact angle hysteresis, and a sliding angle lower than 10° .^[16–19] Superhydrophobicity is based on the so-called Cassie state, where the droplet is supported by a composite surface consisting of solid and air. The frictional forces affecting droplets sliding or rolling on a superhydrophobic surface are the contact angle hysteresis (CAH) force (F_{CAH}) and the viscous dissipating force (F_β).^[20,21] Droplets on superhydrophobic surfaces have low F_{CAH} due to the small three-phase-contact-line-length and the low contact angle hysteresis as caused by the low solid fraction of the surface (liquid is mostly in contact with air, which has no inherent hysteresis). The viscous forces are also reduced by the slip, which has been shown to occur with superhydrophobic surfaces.^[15,22] These factors explain the widely known property of superhydrophobic surfaces of water droplets rolling off at low tilt angles with very little friction. The same friction reduction effect has been exploited for drag reducing in tubes using superhydrophobic inner walls: water flowing or

H. A. Nurmi, C. Yu,^[†] R. H.A. Ras
Department of Applied Physics, School of Science
Aalto University
P.O. Box 15100, Espoo 02150, Finland
E-mail: robin.ras@aalto.fi

D. Toptunov
Neurotar LTD
Viikinkaari 4, Helsinki 00790, Finland

R. H.A. Ras
Department of Bioproducts and Biosystems
School of Chemical Engineering
Aalto University
P.O. Box 16000, Espoo 02150, Finland

V. Jokinen
Department of Chemistry and Materials Science,
School of Chemical Engineering
Aalto University
P.O. Box 16100, Espoo 02150, Finland
E-mail: ville.p.jokinen@aalto.fi

 The ORCID identification number(s) for the author(s) of this article can be found under <https://doi.org/10.1002/admi.202102132>.

© 2022 The Authors. Advanced Materials Interfaces published by Wiley-VCH GmbH. This is an open access article under the terms of the Creative Commons Attribution License, which permits use, distribution and reproduction in any medium, provided the original work is properly cited.

^[†]Present address: Key Laboratory of Bio-inspired Smart Interfacial Science and Technology of Ministry of Education, School of Chemistry, Beihang University, Xueyuan Road 37, Beijing 100191, China

DOI: 10.1002/admi.202102132

droplets rolling, though such tubes do so at reduced friction compared to ordinary hydrophilic or hydrophobic tubes.^[23–27]

However, much less attention has been paid to the possibility of utilizing the low friction properties of superhydrophobic surfaces for lubrication between two solids: superhydrophobic surfaces are inherently rough, whereas smoothness is typically considered to be essential for a good bearing.^[28] Smooth liquid-repellent surfaces have been used in hydrodynamic bearings before to achieve extremely low friction coefficients of 0.0001 for lyophobic surface with hexane^[29] and low coefficients of 0.05 for hydrophobic with 72% aqueous glycerol solution for lubrication.^[30] From the wetting perspective, it has been shown that small frictional forces ($\mu \approx 0.004$) for small velocities ($v < 0.001 \text{ m s}^{-1}$) are possible, which is not typical for the hydrodynamical bearings, which operate typically at velocities larger than 0.1 m s^{-1} .^[31] The tribological properties of dry and submerged superhydrophobic surfaces against steel and tungsten probes have been studied before, and their coefficients of friction have been in the range of $\mu = 0.01\text{--}0.08$.^[32–34] Here, we show that superhydrophobic surfaces used in tandem with hydrophilic surfaces can create a lubricating system based on a water–air bilayer. We achieve superlubricity ($\mu < 0.01$) at low velocities ($v < 0.1 \text{ m s}^{-1}$) with friction coefficient values down to 0.002 with pure water and ambient air as lubricant and under light loads.

2. Results

2.1. Ultra-Low Friction Measurements by Oscillating Tribometry

The lubrication by a water–air-bilayer between a superhydrophobic substrate and a hydrophilic slider (cover glass) with

PDMS cargo is measured using an oscillating tribometer. The oscillating tribometer setup is a slightly modified version of the oscillating droplet tribometer,^[20] in which a hydrophilic slider with magnetic cargo is supported by the water–air-bilayer on the superhydrophobic substrate (Figure 1). The magnetic hydrophilic slider oscillates in between two permanent magnets, and from the decaying amplitude, we can calculate the friction force acting on the substrate. The lubricating bilayer is formed by utilizing the properties of both surfaces: the hydrophilic surface ensures the adhesion and complete spreading of the lubricating water layer, while the superhydrophobic surface is responsible for sustaining the air layer and lowering the friction. The water between the slider and the substrate cannot escape because the adhesion of water to the slider is stronger than the frictional forces and the pressure from the weight of the slider is lower than the Laplace pressure of the lubricating layer (Figure 1c). The superhydrophobic coating used in this work is a commercially available Hydrobead coating, which has advancing and receding contact angles of 166° and 160° , respectively. While we only focus on water and a superhydrophobic surface in this work, the lubricating bilayer can also be formed with liquids other than water and a suitable liquid-repelling surface. This allows for further tuning of the surface tension, viscosity, and evaporation rate.

The frictional forces affecting the superhydrophobic lubricated sliders were measured using the oscillating tribometer,^[20] which calculated the energy dissipating forces based on the decaying harmonic oscillations of a magnetic slider in a harmonic magnetic potential well. This method can be used for any object oscillating on a superhydrophobic surface, as the assumed general harmonic equations hold regardless of the

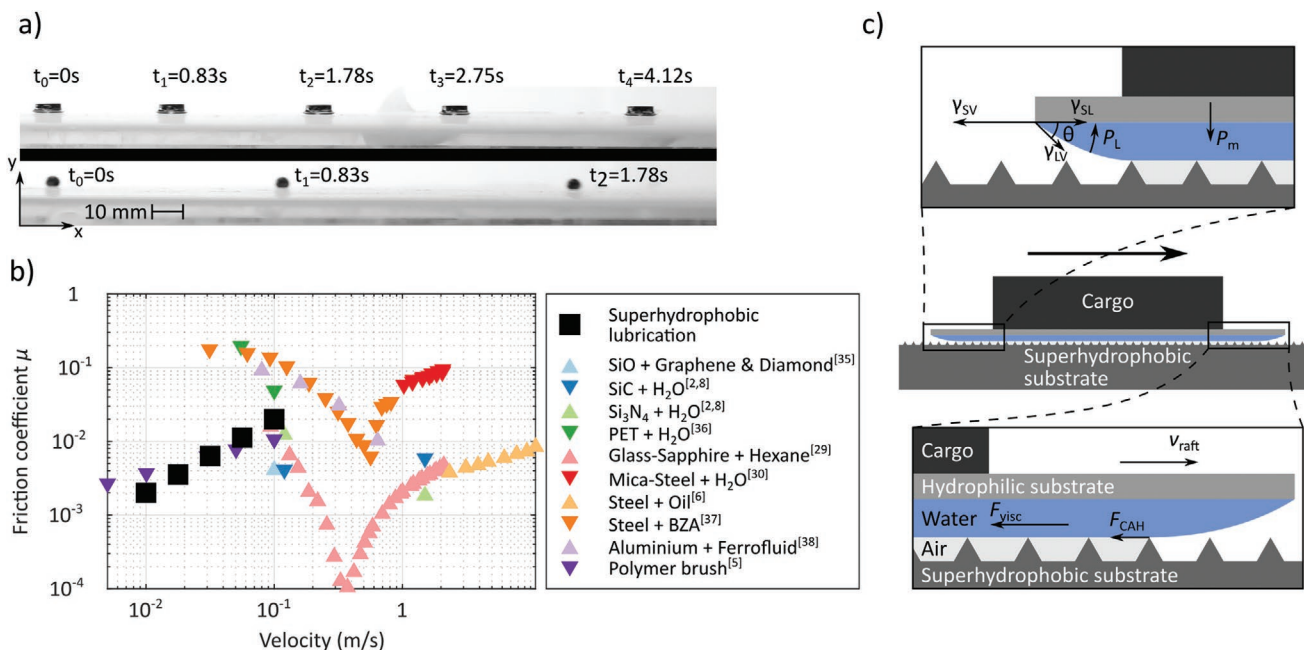


Figure 1. Superhydrophobic lubrication. a) Comparison of a lubricated slider (top) and a water droplet (bottom) on a $0.3^\circ \pm 0.5^\circ$ tilted superhydrophobic surface. b) Comparison of various lubrication methods with superhydrophobic lubrication.^[2,5,6,8,29,35–38] c) Schematic of a model slider comprising a hydrophilic substrate, a superhydrophobic substrate and a water–air bilayer in between them. The weight of the slider and its cargo causes a pressure P_m into the lubricating water layer, while the Laplace pressure P_L of the water lifts the slider. The low contact angle θ of the hydrophilic substrate ensures high adhesion, which holds the lubricating layer under the model slider. γ_{SV} , γ_{SL} , and γ_{LV} are the different interfacial tensions between the phases. The energy dissipating viscous force F_{visc} and contact angle hysteresis force F_{CAH} are shown along with the different parts of the lubrication system.

shape of the oscillating object. The measured frictional forces can be translated into friction coefficient μ_{eff} by comparing the frictional forces to the normal force affecting the model slider

$$\mu_{\text{eff}} = \frac{|F_{\beta}| + |F_{\text{CAH}}|}{mg} = \frac{\beta|\nu| + C_{\text{CAH}}}{mg} \quad (1)$$

where m is the total mass of the slider and g the gravitational acceleration. For these measurements, the CAH force^[39] is assumed to be a constant C_{CAH} with respect to velocity

$$F_{\text{CAH}} = \frac{24}{\pi^3} \gamma D (\cos(\theta_{\text{rec}}) - \cos(\theta_{\text{adv}})) \approx -\text{sign}(\nu) C_{\text{CAH}} \quad (2)$$

where γ is the surface tension of the liquid, D the length of the three-phase contact line where the superhydrophobic solid, liquid, and air meet, and θ_{rec} and θ_{adv} the receding and advancing contact angles. For small contact angle hysteresis forces, it is important to notice that the difference of the cosines must be very small, which means contact angles must be close to each other – much closer than what is reliably possible to measure by contact angle goniometry.^[40,41] The viscous force F_{β} is linearly dependent on velocity and the coefficient scales as with Couette flow

$$F_{\beta} = \beta \nu \propto \frac{A}{h} \nu \quad (3)$$

where β is the coefficient of viscosity, A the contact area of the lubricating film, and h the thickness of the lubricating layer. Based on Equations (2) and (3), the frictional forces depend only on velocity, the geometry, amount of liquid, and the properties of the liquid.

The oscillating tribometer experiments were performed for lubricant volumes of 20–100 μL , slider masses of 131.7–379.0 mg, and slider diameters of 1–3 cm. The lubricant volume and the load effect tests were done with a slider diameter of 1 cm which covers glass weights of 19 mg. The effect of the lubricating volume and the mass and size of the model slider on the friction forces are shown in **Figure 2**. The friction coefficients for the different measurements vary from 0.002 for static friction to 0.01 for dynamic friction ($\nu = 100 \text{ mm s}^{-1}$). The CAH force (1–10 μN) is dominant for static friction, as the viscous force implicates fluids in motion. However, the viscous force dominates the CAH force for the dynamic friction case, because the viscous force grows significantly (3–7 μN) with velocity increase to 10 mm s^{-1} ; details of these effects are shown in Figures S1–S3, Supporting Information.

The effect of lubricant volume can be seen in Figure 2a,d, where the coefficients of friction appear to be constant ($\mu = 0.002 \pm 0.001$, $\mu = 0.04 \pm 0.01$) within error bars for respectively, static and dynamic friction ($\nu = 100 \text{ mm s}^{-1}$). The size of the error bars is partly due to the variability of the different sliders. This can be seen by noting that the error bars in Figure 2a

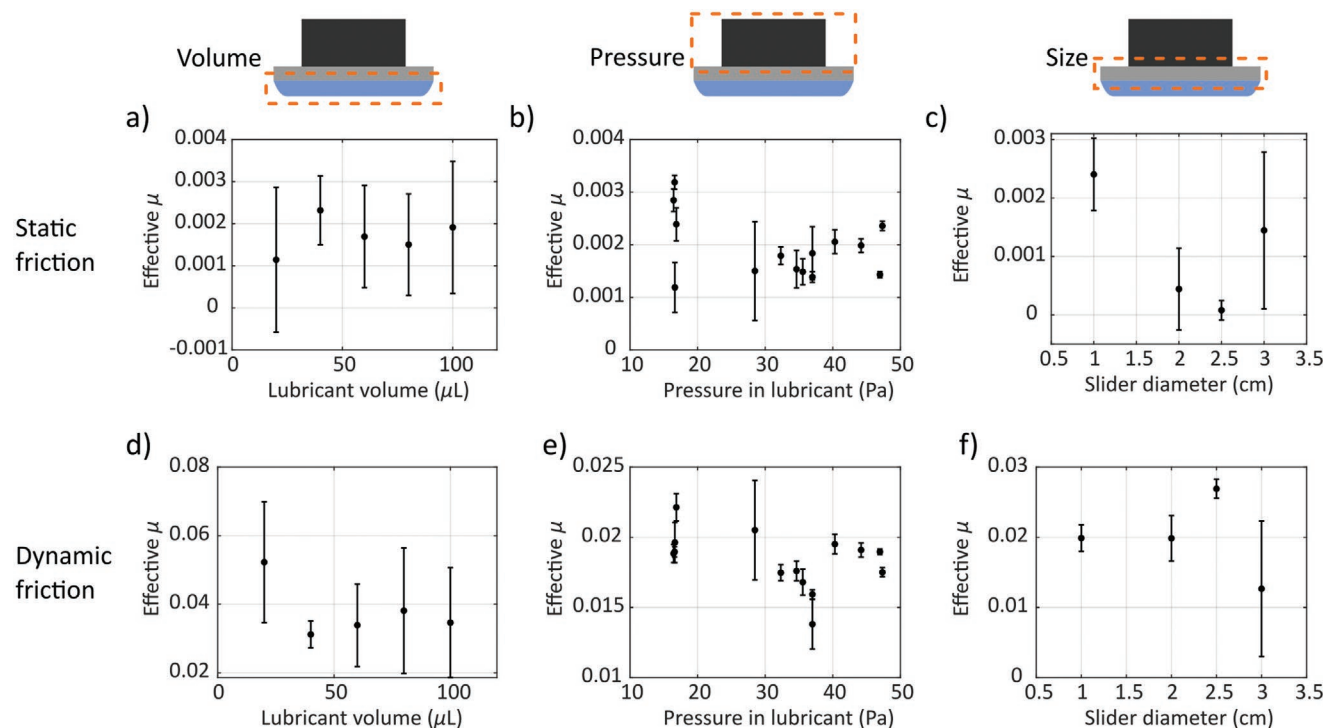


Figure 2. The effect of volume, pressure, and size on the friction coefficient. a) Effect of lubricant volume on static friction coefficient. The data points 20–60, 80, and 100 μL are based on the average of four, three, and two separate sliders, respectively with ten repetitions for each slider. The errors are the standard deviation of the measurements. b) Effect of lubricant pressure on static friction coefficient ($n = 10$). c) Effect of slider size on static friction coefficient (average of four different sliders, $n = 10$ each). Each data point is an average from four different sliders with ten repeated measurements. d) Effect of lubricant volume on dynamic friction coefficient ($\nu = 100 \text{ mm s}^{-1}$) (average of four, three, and two different sliders, respectively, $n = 10$ each). e) Effect of lubricant pressure on dynamic friction coefficient ($\nu = 100 \text{ mm s}^{-1}$) ($n = 10$). f) Effect of slider size on dynamic friction coefficient ($\nu = 100 \text{ mm s}^{-1}$) (average of four different sliders, $n = 10$ each).

which uses averages of multiple different sliders, are roughly an order of magnitude higher than the error bars in Figure 2b, which shows averages of separate measurement with the same slider. As a direct comparison, the 40 μL data point of Figure 2a is the pooled results of the four data points (pressure between 16.4 and 16.9 Pa) of Figure 2b. The lubricant volume has two effects: it increases the thickness of the lubricating layer which decreases the viscous losses in the film based on Equation (3). It also raises the center of mass of the slider system, which makes the slider more labile on top of the lubricating film. Overall, the volume of the lubricating film affects the viscous force, but does not affect the contact angle hysteresis force. The effect of lubricating volume on the coefficient of viscosity and contact angle hysteresis force is shown in Figures S1–S3, Supporting Information. The effect of lubrication layer thickness was also explored with a slider (diameter 1 cm, mass 122.1 mg) by evaporating the lubrication layer (80 μL) over 165 min in ambient conditions (Figure S9, Supporting Information). The static friction coefficient varied from 0.0066 ± 0.0002 to 0.009 ± 0.0003 and the dynamic friction ($v = 0.1 \text{ ms}^{-1}$) from 0.0268 ± 0.0004 to 0.0343 ± 0.0002 . The small increase of the static friction is due to the surface being worn down over 120 oscillations of the slider.

The effect of pressure was explored by increasing the mass of the slider from 131.7 to 379.0 mg keeping constant the lubricant volume (40 μL) and diameter (1 cm). The increased mass does not influence the coefficient of friction as seen in Figure 2b,e. However, the increased mass does linearly increase the contact angle hysteresis force and viscous force (Figures S1–S3, Supporting Information). The maximal load m_{load} for circular sliders allowed by the Laplace pressure can be calculated as

$$m_{\text{load}} = \frac{\pi\gamma}{g} \left(\frac{D}{2} + \frac{D^2}{2\gamma} \right) \quad (4)$$

where D is the diameter of the slider and γ the thickness of the lubricating layer. The derivation of Equation (4) can be found in the Supporting Information. With the given slider parameters ($\gamma = 72.8 \text{ mN m}^{-1}$, $D = 10 \text{ mm}$, and $\gamma \approx 1 \text{ mm}$), the maximum load is calculated to be 1.3 g. However, the lubrication was functional only up to 379.0 mg sliders instead of the theoretical maximum load, which implies there are other factors limiting the load such as the adhesion of the liquid to the hydrophilic substrate. With masses higher than 379.0 mg, the sliders were not lubricated due to tilt leading to one edge of the slider dragging along the superhydrophobic surface and water squeezing out below the slider. By optimizing the slider symmetry, one could potentially achieve the load closer to the estimated maximum load that could be achieved.

The change of lubrication area was explored by imaging the wetted areas of the different mass (135.8 to 378.9 mg) sliders with constant diameter (1 cm) and lubrication volume (40 μL). There is a change of wetted area from 52.33 to 67.25 mm^2 and in lubricant thickness from 0.76 to 0.59 mm (Figure S10, Supporting Information). The effect of this change can be considered only a partial explanation as the viscous coefficient changes much more (167%) as is expected based on Equation (3) (64%).

The tribometer measurements were carried out for four different slider sizes shown in Figure 2c,f. The size of the error

bars is considerable for the 3 cm slider and is likely due to the fact that the slider oscillates only just hindering the accuracy of the analysis. In addition, for two of the 3 cm sliders, the edge of the slider may have touched the superhydrophobic surface in some oscillations, which causes increased friction for those oscillations, increasing the standard deviation of the measurement. The mass of these sliders was selected such that the Laplace pressure in the lubricating layer remains constant. The coefficient of friction stays constant as the slider size increases, showing that at least within this range, the system can be straightforwardly upscaled.

2.2. Tilted Plane Measurements

The friction coefficient was also determined by tilted plane experiment (Figure 3a). These experiments were done with 1–3 cm diameter size slider and the lubricant volume 40–120 μL was scaled to keep the pressure in the lubricant constant (17 Pa). The tilt angle was calculated from the movement of the slider with respect to a plumb line (Figure 3b). This angle is shown for each experiment in Figure S4, Supporting Information. On a tilted plane, the friction coefficient depends on the tilt angle as

$$\mu_{\text{max}} = \tan \alpha \quad (5)$$

where, μ_{max} is friction coefficient of the slider as it moves at terminal velocity and α is the tilt angle of the surface. An example velocity and location of a 2 cm diameter slider is presented in Figure 3c. It shows that the slider has achieved terminal velocity validating the use of Equation (5). The location and velocity profiles for each slider are shown in Figures S5 and S6, Supporting Information. The mean tilt angle was $\alpha = 0.24^\circ \pm 0.1^\circ$, which corresponds to a friction coefficient $\mu \leq 0.004 \pm 0.002$. These values are the mean and standard deviation of all presented measurements shown in Figure 3d. These measurements show that the superhydrophobic lubrication can achieve superlubricity. The tribometer gives the overall friction in oscillating motion with the slider in constant acceleration, whereas the tilting plane experiment measures the case of friction when the velocity is constant. At the terminal velocity, $\approx 7 \text{ mm s}^{-1}$, the frictional forces are the largest and the coefficient of friction can be estimated from the tilt of the plane α according to Equation (5). The viscous forces are similar to the frictional forces at the terminal velocity based on the Equations (3) and (4) and the measured viscous coefficient value.

The results in Figures 3d and 2 show a possibility to upscale the slider size, so we also studied a set of even larger sliders and different geometries to show that the superhydrophobic lubrication effect is robust regarding the size and shape of the surfaces, at least up to the scale of dozens of centimeters. In one example, a circular slider with diameter of 18 cm can lubricate up to 128.3 g of mass, of which 81.4 g is cargo (Video S1, Supporting Information). In another experiment, a transparent slider with mass of 108.7 g and diameter of 35 cm moves easily when the slider is supported by multiple discrete lubricating water droplets instead of by a continuous lubricating water layer (Video S2, Supporting Information). These experiments demonstrate that lubrication is independent of the shape of the lubricating layer as

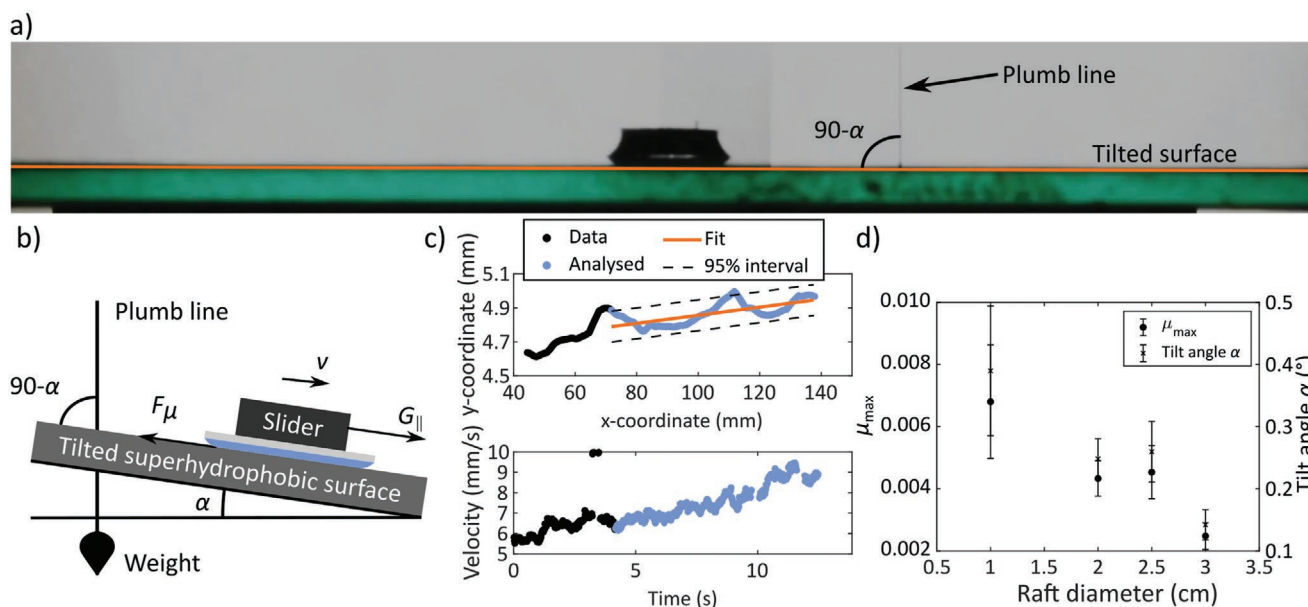


Figure 3. Friction experiment on an inclined plane at ultralow tilt angles ($<0.5^\circ$). a) Motion of a model slider on a superhydrophobic surface tilted by 0.2° . An orange line has been added as a horizontal reference. b) Schematic of the experimental setup that includes a plumb line for accurate determination of tilt angle α . c) Example data set of location and velocity of a 2.5 cm diameter slider. The linear fit of the location data defines the tilt angle. The velocity of the slider in (c) confirms that the slider is moving near to terminal velocity at 9 mm s^{-1} , when the tilt of the surface is small, $\alpha \approx 0.2^\circ$. The velocity and location curves for the other sliders are shown in Figures S5 and S6, Supporting Information. d) Coefficients of friction and tilt angles based on the slider locations and plumb line. This data shows similar coefficients of friction as with the oscillating tribometer. The error bars correspond to the 95% confidence interval of slope of the slider path.

long as there is sufficient lubrication. The supplementary videos (Videos S1 and S2, Supporting Information) show both linear and rotational lubrication on a flat surface proving the concept-of-experiment. The lubrication should also work for typical bearing types (journal, linear, and thrust) and curved surfaces if the liquid adheres strongly enough on the slider and forms the bilayer.

2.3. Tunable Lubrication

We demonstrate that superhydrophobic lubrication allows to be dynamically adjusted by adding and removing tap-water after placing the hydrophilic slider on the superhydrophobic substrate (Figure 4a). The lubricating water is supplied and removed through the holes in the superhydrophobic coating on an air lubrication stage (Figure S7, Supporting Information). The increased pressure causes water droplets to bead from the holes in the superhydrophobic substrate as shown in Video S2, Supporting Information. The lubrication can be reversibly switched on and off by controlling the amount of water between the two surfaces which is shown in Video S3, Supporting Information. This control was done by increasing and decreasing the pressure in the water storage. Similarly, the decreased pressure causes the water beads to flow back into the storage.

2.4. Application as 2D Mouse Treadmill

Superhydrophobic lubrication was tested as a replacement for the air lubrication used in Neurotar's Mobile HomeCage

(Figure 4b).^[42] The cage (mass 46.9 g) provides support for a mouse (mass 20–25 g) to keep its head stationary for neuroimaging while the mouse is awake and active, by allowing the cage to move freely and nearly frictionlessly under the mouse (to enable in mouse's perception that the mouse moves inside the cage). The cage with deionized water underneath was placed on a superhydrophobic surface of $\approx 30 \text{ cm}$ by 30 cm . A demo experiment of the superhydrophobic lubrication with cage is shown in Figure 4b; and Video S4, Supporting Information. Compared to air lubrication, the superhydrophobic lubrication is quieter and passive, which improves the neuroimaging conditions by keeping the mouse as stress-free as possible.

3. Conclusion

We have demonstrated a water–air lubrication system, which is completely passive and achieves superlubricity with friction coefficients of $\mu = 0.002 \pm 0.001$ at a pressure of 50 Pa and at a velocity less than 10 mm s^{-1} , which was confirmed by both oscillating tribometer and tilting plane experiments. We note that a straightforward way of lowering the friction further would be to utilize a superhydrophobic surface with an even lower contact angle hysteresis than the Hydrobead coating used in this work. This would directly lower the contact angle hysteresis force and possibly, also induce more slip to reduce the viscous forces. Previous lubrication research has mostly focused on surfaces having smooth surfaces^[13] and rough surfaces have often been found to be suboptimal compared to smooth surfaces.^[28] However, we show here that a rough superhydrophobic

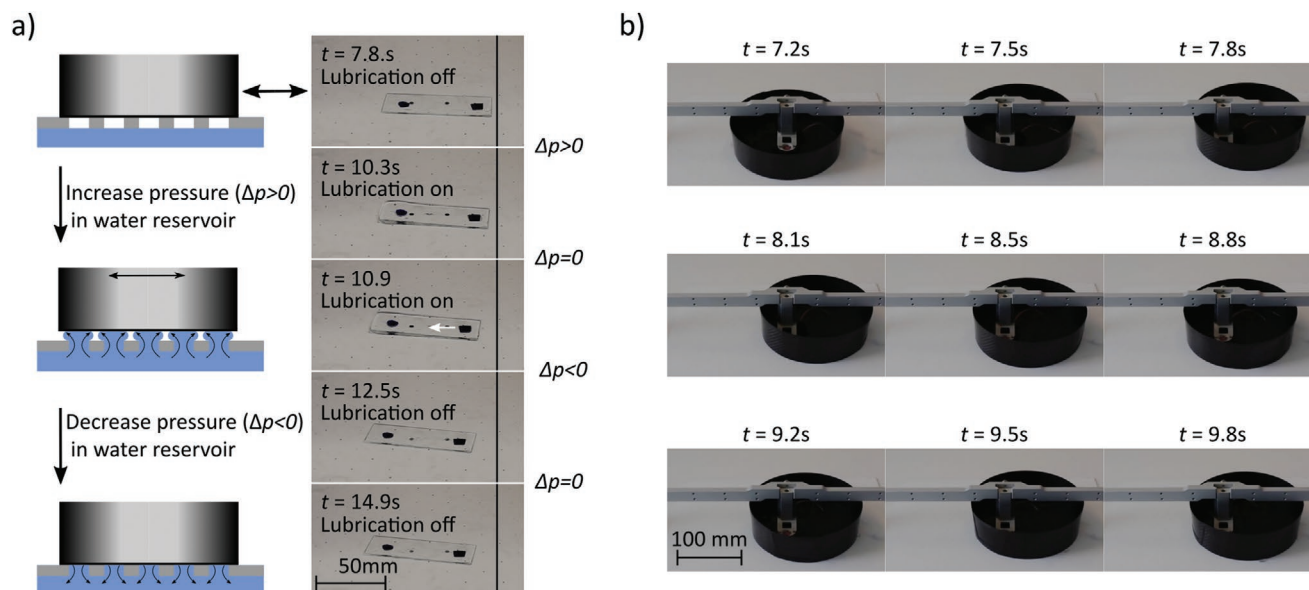


Figure 4. Applications of superhydrophobic lubrication. a) Tunable lubrication. Schematic and time series of a dynamically tunable lubrication system using a microscope slide as slider on a superhydrophobic substrate with an array of mm-sized holes. Snapshots taken from Video S3, Supporting Information. Large black dots at each side of the microscope slide and the black line are included as reference of the position. The lubrication can be turned on by increasing pressure in the water reservoir forcing water under the slider, and can be turned off by decreasing the pressure, letting water back to the reservoir and thereby removing water from under the slider. The surface tilt angle is 0.7° , which is sufficient for the slider to move. b) Time series of superhydrophobic lubrication system with the Mobile HomeCage with a mouse. The time series is from Video S4, Supporting Information, where mouse can move the cage freely due to low friction of the superhydrophobic lubrication.

surface in tandem with a hydrophilic surface exhibits superlubricity by forming a lubricating bilayer of water and air. The rough surface and air form a smooth interface with liquid-slip decreasing the frictional forces. The achieved lubrication compares favorably with conventional lubrication methods in the low-velocity domain (Figure 1b).

In addition, we have shown possible applications for this kind of lubrication as tunable lubrication and a mouse cage for neuroimaging with superhydrophobic lubrication. In these applications, we have shown that superhydrophobic lubrication works with different sizes and shapes. Overall, this novel lubrication method could inspire improvements for green lubrication as well as refocus lubrication research to also include highly liquid-repellent surfaces.

4. Experimental Section

Superhydrophobic Surface Fabrication: The superhydrophobic coatings were made using commercial Hydrobead coating. The microscope glass was cleaned by sonicating in 10%-Deconex solution for 5 min. Then, the glass was rinsed with deionized water and dried with nitrogen flow. The glass was spray coated with Hydrobead and left to dry for minimum 2 h. For larger glass panels, the cleaning was done by manual washing with hot water and detergent. Then, the panel was rinsed with deionized water and dried with nitrogen flow. The panel was then spray coated with Hydrobead and left to dry for minimum 2 h.

Oscillating Tribometer: The oscillating tribometer measures the forces affecting the model slider as it oscillates in harmonic potential created by two permanent magnets separated from each other by 3 cm (Figure S8, Supporting Information). The two magnets are connected to a linear stage (Aerotech PRO165LM), which is moved in a sinusoidal way for two oscillations, causing the slider to oscillate. The slider's motion follows

the equation of a general harmonic oscillator with viscous and contact angle hysteresis force:

$$ma = -kx - \beta v - \text{sign}(v)F_{\text{CAH}} \quad (6)$$

Here m is the mass of the droplet, a acceleration of the slider, k spring coefficient due to magnetic forces, x displacement of the slider from magnets axis, β viscous coefficient, v velocity of the droplet, and F_{CAH} the contact angle hysteresis force. The parameters k , β , and F_{CAH} were solved by fitting the measured slider location with the analytical solution of Equation (6).^[43] The solution of the general harmonic oscillator is a piecewise solution for each half-oscillation n as

$$x(t) = x\left(\frac{nT}{2} + \tau\right) = x_{n+1}(\tau) \quad (7)$$

where

$$x_{n+1} = (-1)^n A_0 \left\{ \sqrt{1 + \tilde{\beta}} \left[(1 + \tilde{F}) e^{-\tilde{\beta}\pi n} - 2\tilde{F} \sum_{j=0}^n e^{-\tilde{\beta}\pi j} \right] e^{-\tilde{\beta}\omega\tau} \cos\left(\omega\tau - \cos^{-1}\left(\frac{1}{\sqrt{1 + \tilde{\beta}}}\right)\right) + \tilde{F} \right\} \quad (8)$$

where A_0 is the starting amplitude, ω the angular frequency of the oscillation, $\tilde{F} = \frac{F_{\text{CAH}}}{kA_0}$ the dimensionless sliding friction, and $\tilde{\beta} = \frac{\beta}{\omega m}$, the dimensionless viscous dissipation coefficient.^[20]

A high-speed camera (Phantom v1610) captured the motion of the model slider with 1000 fps, and a custom MATLAB code obtained the location of the slider from the recorded video. The MATLAB code analyzes each frame by cropping the frame at the liquid–solid interphase and above the slider, and thresholding the grayscale image into binary black-and-white frame. The centroid of the slider can be obtained from this black-and-white frame (Figure S8b, Supporting Information). The centroid location data was fitted into the analytical solution of Equation (6) by the least squared method to obtain the oscillation parameters k , β , and F_{CAH} .

The magnetic horizontal force is zero, when the horizontal distance to the magnets is equal (15 mm). The force affecting the paramagnetic particles in vertical and horizontal direction can be estimated from equations $F_{(m,z)} = \mu_0 V \left(M + H \frac{dM}{dH} \right) \frac{dH}{dz}$ and $F_{(m,x)} \approx -\mu_0 V c \left(M + H \frac{dM}{dH} \right) x$, where μ_0 is the permeability of space, V volume of ferrofluid droplet, M magnetization of the particles, H magnetic field strength, $\frac{dM}{dH}$ is gradient of magnetization of ferrofluid droplet as a function of the magnetic field, $\frac{dH}{dz}$ is gradient of the magnetic field in vertical direction, c is field curvature in horizontal direction, and x is the horizontal coordinate of the ferrofluid droplet.^[20] The magnetic force depends on the amount of paramagnetic particles in the slider or the ferrofluid droplet, thus the magnetic force acting on the slider can be estimated with a ferrofluid droplet with the same amount of paramagnetic particles. This estimation was done by calculating the volume of a ferrofluid droplet with the same spring coefficient k , and then using the force affecting such a droplet as the estimate of the magnetic force affecting the slider in an arbitrary place around the two-magnet setup. The vertical magnetic force as the slider is 14 mm from the upper magnet and 16 mm from the lower magnet is 236 μN toward the upper magnet. This force was much lower than the gravitational normal force of even the lightest slider, which was 1373 μN .

Slider Manufacturing: The slider consisted of hydrophilic substrate (cover glass) and PDMS cargo. To make cargo for the model sliders, 10:1 ratio of PDMS (Sylgard-184) was mixed, degassed in vacuum, poured into the template with a PMMA rod of 2.5 mm diameter concentric to the template, and cured in an oven for 90 min at 70 °C. For extra mass, copper powder of mesh 100 was added at the ratio of 1:1 by mass. The cover glass was connected concentrically to the partially cured PDMS with a droplet of PDSM in the middle of the curing. After curing, a rod of PMMA was removed to form a hole into which 3 μL of concentrated ferrofluid with iron oxide nanoparticles was added. The ferrofluid was dried and then sealed inside the slider with a piece of paper and PDMS, which was cured.

Tribometer Measurement Protocol: The sliders were prepared by cleaning the bottom of the slider with oxygen plasma for 5 min, rendering the bottom hydrophilic. This way, the water wet the whole bottom surface of the slider preventing the water from escaping between the slider and surface. After the plasma cleaning, the slider was stored with its bottom wetted with water to keep the bottom of the slider hydrophilic. As the slider was placed on the measurement setup, the slider was dried with lint-free paper and a set amount of lubrication water was added to the bottom with Finnipipette. The magnets of the setup oscillated with an amplitude of 4 mm, frequency of 3 Hz, and two times to make the slider move. With this setup, the slider achieved 8 mm maximum amplitude, which then decayed over 2 s. A high-speed camera recorded the movement of the slider from which the location of mass center was analyzed from the side profile of the slider after turning the grayscale image into a black-and-white image. The acquired location contained information about the oscillation parameters k , β , and CCAH, which were extracted by fitting the analytical model to the data by nonlinear least squares method.

Tilted Plane Measurement Protocol: The tilted plane measurement was done by placing the model slider with a set amount of lubricant by volume at the higher side of the pre-tilted plane with tweezers. The movement of the slider was recorded by Canon D60 camera, which was rotated by roughly 30° to increase the location resolution in the direction of gravity and the movement of the slider. This was done because the differences in the height of the slider were in the order of a pixel and the swinging motion of the plumb weight was similarly, in the order of a pixel. The direction of the plumb line was analyzed by thresholding the video and analyzing the direction by MATLAB's regionprops function. The location of the slider was obtained by finding the centroid of the moving slider by MATLAB's regionprops function after thresholding the video. The velocity was calculated from the 2D location data and the frame rate. The tilt angle of the surface was calculated by computing

the difference of the direction of the plumb line and the angle of incline of the slider's movement.

Tunable Superhydrophobic Lubrication Stage: The tunable superhydrophobic lubrication stage is an air lubrication stage with a superhydrophobic coating. The inside of the stage was filled with tap water and the pressure in the stage was controlled by changing the height of the filling tube of the stage. The height difference between the stage surface and the water level in the filling tube caused a pressure difference in the water, which was utilized to tune the lubrication.

Lubrication of Neurotar Mobile HomeCage: The cage with mouse was placed on the superhydrophobic surface, and the mouse's head was fixed in the metal clamp. Deionized water was added until the mouse cage was lubricated. The movement of the mouse was observed and recorded with a camera. This experiment was done in accordance with the animal licence ESAVI/31282/2019 issued by ELLA (Eläinkoelautakunta).

Supporting Information

Supporting Information is available from the Wiley Online Library or from the author.

Acknowledgements

This work was supported by the Academy of Finland (Centres of Excellence Programme (2014–2019)). R.H.A.R. acknowledges the European Research Council for funding the Consolidator Grant SuperRepel (grant agreement no. 725513). The authors acknowledge the provision of facilities by Aalto University at OtaNano – Micronova Nanofabrication Centre.

Conflict of Interest

The authors declare no conflict of interest.

Data Availability Statement

The data that support the findings of this study are available from the corresponding author upon reasonable request.

Keywords

green tribology, hydrophilic surfaces, superhydrophobic lubrication, water lubricants, water repellent

Received: November 1, 2021
Revised: November 23, 2021
Published online: January 5, 2022

- [1] P. A. Tipler, G. Mosca, *Physics for Scientists and Engineers*, W. H. Freeman and Company, New York, NY **2003**.
- [2] V. Ferreira, H. N. Yoshimura, A. Sinatora, *Wear* **2012**, 296, 656.
- [3] M. V. S. Babu, A. R. Krishna, K. N. S. Suman, *Am. J. Mater. Sci. Technol.* **2015**, 4, 72.
- [4] M. Chen, W. H. Briscoe, S. P. Armes, J. Klein, *Science* **2009**, 323, 1698.
- [5] H. Arafune, T. Kamijo, T. Morinaga, S. Honma, T. Sato, Y. Tsujii, *Adv. Mater. Interfaces* **2015**, 2, 1500187.

- [6] S.-C. Vladescu, N. Marx, L. Fernández, F. Barceló, H. Spikes, *Tribol. Lett.* **2018**, *66*, 127.
- [7] M. Chen, K. Kato, K. Adachi, *Tribol. Lett.* **2001**, *11*, 23.
- [8] S. Yan, B. Lin, F. Liu, F. Yan, *Int. J. Precis. Eng. Manuf.* **2012**, *13*, 1067.
- [9] M. Nosonovsky, B. Bhushan, *Philos. Trans. R. Soc., A* **2010**, *368*, 4677.
- [10] Z. Xie, Z. Rao, Ta-Na, L. Liu, R. Chen, *Mech. Ind.* **2016**, *17*, 106.
- [11] B. M. Ginzburg, D. G. Tochil'nikov, V. E. Bakhareva, A. V. Anisimov, O. F. Kireenko, *Russ. J. Appl. Chem.* **2006**, *79*, 695.
- [12] Z. Xie, Z. Rao, H. Liu, *Coatings* **2019**, *9*, 23.
- [13] M. Z. Baykara, M. R. Vazirisereshk, A. Martini, *Appl. Phys. Rev.* **2018**, *5*, 041102.
- [14] J. P. Rothstein, *Annu. Rev. Fluid Mech.* **2010**, *42*, 89.
- [15] C. Lee, C.-H. Choi, C.-J. Kim, *Phys. Rev. Lett.* **2008**, *101*, 064501.
- [16] M. Liu, S. Wang, L. Jiang, *Nat. Rev. Mater.* **2017**, *2*, 17036.
- [17] N. J. Shirtcliffe, G. McHale, S. Atherton, M. I. Newton, *Adv. Colloid Interface Sci.* **2010**, *161*, 124.
- [18] T. Mouterde, P. S. Raux, C. Clanet, D. Quéré, *Proc. Natl. Acad. Sci. U.S.A.* **2019**, *116*, 8220.
- [19] X. Tian, T. Verho, R. H. A. Ras, *Science* **2016**, *352*, 142.
- [20] J. V. I. Timonen, M. Latikka, O. Ikkala, R. H. A. Ras, *Nat. Commun.* **2013**, *4*, 2398.
- [21] M. Backholm, D. Molpeceres, M. Vuckovac, H. Nurmi, M. J. Hokkanen, V. Jokinen, J. V. I. Timonen, R. H. A. Ras, *Commun. Mater.* **2020**, *1*, 64.
- [22] Y. C. Jung, B. Bhushan, *ACS Nano* **2009**, *3*, 4155.
- [23] C.-H. Choi, U. Ulmanella, J. Kim, C.-M. Ho, C.-J. Kim, *Phys. Fluids* **2006**, *18*, 087105.
- [24] J. J. Yuan, R. H. Jin, *Nanotechnology* **2010**, *21*, 065704.
- [25] N. J. Shirtcliffe, G. McHale, M. I. Newton, Y. Zhang, *ACS Appl. Mater. Interfaces* **2009**, *1*, 1316.
- [26] S. Hoshian, E. Kankuri, R. H. A. Ras, S. Franssila, V. Jokinen, *Sci. Rep.* **2017**, *7*, 16019.
- [27] M. Vuckovac, M. Backholm, J. V. I. Timonen, R. H. A. Ras, *Sci. Adv.* **2020**, *6*, eaba5197.
- [28] R. Haque, S. K. Guha, *Proc. Inst. Mech. Eng., Part C* **2005**, *219*, 1249.
- [29] J. H. Choo, R. P. Glovnea, A. K. Forrest, H. A. Spikes, *J. Tribol.* **2007**, *129*, 611.
- [30] J. H. Choo, H. A. Spikes, M. Ratoi, R. Glovnea, A. Forrest, *Tribol. Int.* **2007**, *40*, 154.
- [31] K. Hiratsuka, A. Bohno, H. Endo, *J. Phys.: Conf. Ser.* **2007**, *89*, 012012.
- [32] Y. Guo, Y. Zhu, C. Li, B. Luo, Z. Lv, K. Li, *Lubr. Sci.* **2021**, *33*, 246.
- [33] Y. Wan, Z. Wang, Z. Xu, C. Liu, J. Zhang, *Appl. Surf. Sci.* **2011**, *257*, 7486.
- [34] T. J. Young, J. Jackson, S. Roy, H. Ceylan, S. Sundararajan, *Wear* **2017**, *376–377*, 1713.
- [35] D. Berman, S. A. Deshmukh, S. K. R. S. Sankaranarayanan, A. Erdemir, A. V. Sumant, *Science* **2015**, *348*, 1118.
- [36] T. D. Nguyen, J. Sukumaran, J. De Pauw, P. De Baets, *Int. J. Sustain. Constr. Des.* **2013**, *4*, <http://ojs.ugent.be/SCAD/article/view/1048>.
- [37] S. Zhang, C. Zhang, K. Li, J. Luo, *RSC Adv.* **2018**, *8*, 9402.
- [38] W. Huang, C. Shen, S. Liao, X. Wang, *Tribol. Lett.* **2011**, *41*, 145.
- [39] A. I. ElSherbini, A. M. Jacobi, *J. Colloid Interface Sci.* **2006**, *299*, 841.
- [40] K. Liu, M. Vuckovac, M. Latikka, T. Huhtamäki, R. H. A. Ras, *Science* **2019**, *363*, 1147.
- [41] M. Vuckovac, M. Latikka, K. Liu, T. Huhtamäki, R. H. A. Ras, *Soft Matter* **2019**, *15*, 7089.
- [42] M. Kislin, E. Mugantseva, D. Molotkov, N. Kuleskaya, S. Khirug, I. Kirilkin, E. Pryazhnikov, J. Kolikova, D. Toptunov, M. Yuryev, R. Giniatullin, V. Voikar, C. Rivera, H. Rauvala, L. Khiroug, *J. Visualized Exp.* **2014**, *29*, e51869.
- [43] A. Ricchiuto, A. Tozzi, *Am. J. Phys.* **1982**, *50*, 176.